

Amino-functionalized mesoporous nano-silica/polyvinylidene fluoride composite as efficient ultrafiltration membrane

Heba Abdallah^a, Marwa S. Shalaby^{a,*}, Antonio Buonerba^{b,c}, Ahmed M. Shaban^d, Laura Borea^b, Tiziano Zarra^b, Vincenzo Belgiorno^b, Vincenzo Naddeo^b

^aChemical Engineering and Pilot Plant Department, Engineering Research Division, National Research Centre, 33 El Bohouth Street (Former El Tahrir Street), P.O. Box: 12622, Dokki, Giza, Egypt, Tel. 202 33335494; Fax: 202 33370931; emails: marwashalaby_4@yahoo.com (M. Shalaby), heba_nasr94@yahoo.com (H. Abdallah)

^bSanitary Environmental Engineering Division (SEED), Department of Civil Engineering, University of Salerno, Via Giovanni Paolo II, 132, 84084 Fisciano, Salerno, Italy, Tel. +39 089969333; emails: abuonerba@unisa.it (A. Buonerba), lborea@unisa.it (L. Borea), tzarra@unisa.it (T. Zarra), v.belgiorno@unisa.it (V. Belgiorno), vнадdeo@unisa.it (V. Naddeo)

^cInterUniversity Centre for the Prediction and Prevention of Major Hazards, Via Giovanni Paolo II, 84084 Fisciano, Salerno, Italy

^dWater Pollution Research Department, National Research Centre, 33 El Bohouth Street (Former El Tahrir Street), P.O. Box: 12622, Dokki, Giza, Egypt, email: ashaban12311@gmail.com (A.M. Shaban)

Received 25 February 2020; Accepted 24 July 2020

ABSTRACT

Ultrafiltration mixed matrix membranes were prepared using polyvinylidene fluoride (PVDF) with functionalized mesoporous amino nano-silica (NS). The prepared functionalized mesoporous amino nano-silica (NS) was characterized using X-ray diffraction, transmission electron microscopy, and Fourier transform infrared. The results indicate that the addition of amino-functionalized nano-silica improves the hydrophilicity of the membrane. Membranes M5 and M6 showed the highest tensile properties. M5 showed a tensile strength of 82.5 kg/m² and elongation of 25.5%, while the tensile strength of 87.9 kg/m² and an elongation of 29.3% were found for M6. M6 exhibited an optimal morphology due to the formation of a small dense top layer and a wide finger-like sublayer, affording a permeate flux 347 L/m²h and a rejection of 98.8% for humic acid concentration 3 g/L. M5 exhibited a more compact spongy-like structure, with a permeate flux of 294 L/m²h and rejection of 99.7% for humic acid at concentration 3 g/L. The bovine serum albumin (BSA) was used also as a feed solution in the performance testing, using a feed concentration of 3 g/L. M5 and M6 showed the highest removal percentage for BSA of 99.5% and 99.2%, respectively. The fouling test was carried out using humic acid solutions (10 g/L) and BSA solution (3 g/L). M5 and M6 showed excellent antifouling properties, where F_{RR} of M5 and M6 were, respectively, of 99.71% and 99.43% for humic acid solution, while F_{RR} for M5 and M6 were, respectively, of 98.5% and 97.96% for BSA solution.

Keywords: Ultrafiltration; Blend membranes; Polyvinylidene fluoride; Mesoporous amino nano-silica

1. Introduction

Commonly used ultrafiltration polymeric membranes are based on polyvinylidene fluoride (PVDF), which has

been used for various kinds of wastewater remediations [1]. The problem associate with the use of this type of membranes is the hydrophobicity, which facilitates the fouling of membrane leading to bad membrane performance. Recent investigations attempted to improve surface hydrophilicity in order

* Corresponding author.

to enhance membrane performance. Many different methods can be used, including chemical grafting, chemical blending, and surface modification. Blending with different kinds of nanoparticles provides an improvement in membranes performance [1,2]. Blending techniques are cost-effective ways to improve the properties of the membrane. The thermodynamic behavior in terms of mass and heat transfer plays an important role in the compounding processes of polymeric membrane. Heat and mass transfer provide the miscibility gap at a certain temperature and composition according to polymer-polymer interaction [3,4]. The interaction between polymers depends on solvent diffusion and in turn on polymer chains disentanglement. This process is governed by the Gibbs free energy (ΔG) of mixing, governed by both enthalpic and entropic factors [5–7]. Negative ΔG indicates complete miscibility of polymer and solvent. The mixing of high molecular weight polymers in a solvent is typically associated with a small change in entropy therefore, enthalpy is the major factor affecting the ΔG [5–7]. The thermodynamic of mixing of polymer with nanoparticles, like PVDF and nano-silica, depends on the degree of dilution. High concentration of polymer can affect solubility, affording positive Gibbs free energy. Low concentration of polymer and a concentration of nano-silica less than 50% under sonication conditions, typically assures negative ΔG values, because the nanoparticles are suspended in the polymeric solution during mixing [3–6].

The inclusion in polymer membranes of TiO_2 , SiO_2 , or CaCO_3 nanoparticles, graphene, or carbon nanotubes can lead to an enhancement of the antifouling properties [3,4]. For example, some researchers studied the blending of polyethersulfone (PES) with inorganic nanoparticles improving the membrane performance [3]. The preparation of PES membranes with titanium dioxide nanotubes, PES/ TiO_2 NTs, afforded for 8,000 ppm brackish water a salt rejection of 99% and a permeate flux of 18.2 $\text{kg/m}^2\text{h}$ [3]. The blending of PES with manganese acetylacetonate nanoparticles afforded osmosis membranes with a salt rejection for seawater of 99% [6]. Membranes with good mechanical properties were obtained by blending PVDF with silica nanoparticles coated with graphene oxide [8].

Most commercial membranes are produced by supporting the filtering material onto polyester fibers as a non-woven support. The support enhances the membrane strength, additionally limiting the shrinkage of membranes during preparation [9,10].

The membrane surface charge is one of the most important factors which can affect the membrane antifouling properties. The separation performance of charged membranes depends on the effect of steric sieve and on charge repulsion [11]. According to the charge on the membrane surface, the kind of wastewater removable is determined by the foulant charge. For example, to remove pollutant dyes from textile wastewater, such as methyl orange and Congo red, the membrane should have a negative charge because these dyes have the same charge, in order to prevent the adsorption onto membrane surface that could produce the fouling [12]. Membranes with positive surface charge were developed by grafting poly(*N,N*-dimethylaminoethyl methacrylate) on polyvinylchloride (PVC) for the removal of multivalent cations, such as calcium, magnesium, chromium, and lead from wastewater as well as drinking water [13]. It

is generally accepted that the use of surface charged membranes improves selective electrostatic repulsion between foulant and membrane surface, thus preventing membrane fouling [14–16]. Electronegative charged membrane will lead to inhibited protein adsorption with improved antifouling property. Moreover, the fabrication of hydrophilic and negatively charged membranes, with high antifouling properties, was obtained by electrospinning of nanofibre [16]. Those membranes were found efficient for microfiltration of water and wastewater containing hard oily foulants.

In this work, we report preparation and development of novel ultrafiltration supported membranes with antifouling properties. The membranes were obtained by compounding polyvinylidene fluoride with functionalized mesoporous amino nano-silica and subsequent casting onto both woven and non woven supports. The prepared membranes exhibit charged surfaces with improved antifouling properties. The influence of the functionalized mesoporous amino nano-silica was studied in order to evaluate the effectiveness in ultrafiltration of water. The prepared membranes were characterized by using several analytical methods.

2. Experimental section

2.1. Materials

Tetraethylorthosilicate (TEOS, Sigma-Aldrich, Egyptian International Center for Import in Cairo, Egypt), cetyltrimethylammonium bromide (CTABr, 99%, Sigma-Aldrich, Egyptian International Center for Import in Cairo, Egypt), sodium hydroxide (Merck, Egyptian International Center for Import in Cairo, Egypt), 3-aminopropyltriethoxysilane (Merck, Egyptian International Center for Import in Cairo, Egypt), 3-[2-(2-aminoethylamino) ethylamino]propyltrimethoxysilane (Sigma-Aldrich, Egyptian International Center for Import in Cairo, Egypt), polyvinylidene fluoride powder (PVDF, M_w 534,000, Sigma-Aldrich, Egyptian International Center for Import in Cairo, Egypt), polyethylene glycol (PEG 400, Fluka, Egyptian International Center for Import in Cairo, Egypt), *N*-methyl-2-pyrrolidone (NMP, Sigma-Aldrich, Egyptian International Center for Import in Cairo, Egypt), dodecyl amine (Fluka, Egyptian International Center for Import in Cairo, Egypt), humic acid (Roth Indian Company, Imported from India), bovine serum (Roth Indian Company, Imported from India), hydrochloric acid (Merck, Egyptian International Center for Import in Cairo, Egypt), sodium nitrate (Merck, Egyptian International Center for Import in Cairo, Egypt), absolute ethyl alcohol (EtOH, Sigma-Aldrich, Egyptian International Center for Import in Cairo, Egypt), and toluene (Merck, Egyptian International Center for Import in Cairo, Egypt), unless otherwise stated, were used as received without further purification.

2.2. Procedure for membrane preparation

2.2.1. Preparation of nano-silica functionalized with amine groups

Mesoporous silica was prepared according to a conventional hydrothermal method [8]. TEOS and CTAB were used respectively as a silicon source and a template. TEOS (0.65 M) was added drop-by-drop under stirring to 0.42 g of CTABr dissolved in a solvent mixture of EtOH/ H_2O heating up to 343 K for 1 h. The molar ratio $\text{SiO}_2/\text{CTABr}/\text{Na}_2\text{O}/$

EtOH/H₂O of the resulting gel was 1.4:1:0.35:5:140. The gel was transferred into Teflon-lined stainless-steel autoclaves and was heated in oven at 373 K for 4 d. The product was filtered, washed, calcined in air at a heating rate of 1 K/min, and thermostated at a final temperature of 813 K for 6 h. Three hundred milligrams of mesoporous silica powder was dispersed in toluene (15 mL) under a protective atmosphere of argon under stirring for 15 min after that 650 mL of amine silane agent was added at 383 K by heating in an oil bath for 1 h under stirring. The produced solid was filtered and washed using dichloromethane/diethyl ether (1:1) mixture, the solid was dried at 323 K for 12 h.

2.2.2. Preparation of UF membranes

PVDF membranes were produced by phase inversion method. Different polymeric suspensions were prepared using a variable percentage of a nano-silica solution as depicted in Table 1. Nano-silica suspension was prepared by dissolving different percentages of nano-silica (0.1, 0.3, and 0.5 g) with 2 g; dodecyl amine in 10 g ethanol under sonication for 1 h. Two percent of that suspension was added to the polymer solution with PEG and the mixing process was carried out for 8 h. The polymeric solution was cast onto woven or nonwoven polyester supports to study the effect of support on membrane performance. Prepared membranes on different supports were fixed on glass plates which were subsequently immersed in a water gelation bath.

2.3. Instrumentation and methods

X-ray diffraction (XRD) patterns were recorded at scanning rate of 5 s/step with a Philips X' Pert (importers in Egypt) multipurpose diffractometer (MPD). Transmission electron microscopy (TEM) imaging was performed with FEI-TECNAI T20 TEM microscope at 200 kV. Fourier transform infrared (FTIR) spectra of as prepared samples were acquired with a Bruker Vertex 70 FTIR spectrometer (through Agilent Scientific Instruments and their agency in Egypt) at resolution of 2 cm⁻¹ by collecting a number of 100 scans in the wavenumber range of 4,000–600 cm⁻¹. Scanning electron microscopy (SEM) imaging was performed with JEOL 5410 microscope at voltage of 10 kV. The samples were electrospun with a thin layer of gold prior to analysis. Tensile properties were determined with a H5KS universal tensile testing machine equipped with a tensile load cell of 5 N. The measurements were carried out at room temperature with cross-head speed of 30 mm/min and gauge length of 100 mm, of specimens (length 200 mm and width of 25 mm) produced by die-cutting of membranes. The test was repeated three times for each sample. Membrane porosity was estimated with the following equation [5,6], determining the weight of the membrane dried at 80°C for 24 h, and of the same after soaking in water and draining excess of water with filter paper.

$$\varepsilon = \frac{W_0 - W_1}{V} = \frac{W_0 - W_1}{A \cdot \delta} \quad (1)$$

where ε is the membrane porosity; W_0 and W_1 are the weights (in gram) of wet and dry membranes, respectively; V is the membrane volume, where A is surface area (in m²) and δ

Table 1
Preparation of PVDF/NS UF membranes

Membrane ID ^a	Support	NS (%)
M1	Woven	–
M2	Nonwoven	–
M3	Woven	0.1
M4	Nonwoven	0.1
M5	Woven	0.3
M6	Nonwoven	0.3
M7	Woven	0.5
M8	Nonwoven	0.5

^aComposition of polymer-silica suspensions for casting onto woven and nonwoven support: NMP (78 wt.%), PVDF (18 wt.%), PEG (2 wt.%), and NS suspended in dodecyl amine/ethanol solvent mixture.

the thickness (in m). Membrane thickness was measured with a micrometer screw gauge. The test was repeated three times for each sample. Internal surface area of supported and unsupported membrane blends was determined using Brunauer–Emmett–Teller (BET) method with a Chem BET-3000 apparatus from Quantachrome [17,18]. The samples were cut in strips, placed in a glass column, dried, and degassed by heating at 80°C for 3 h. Adsorption and desorption cycles were carried out on with nitrogen. Contact angle measurements were carried out with a compact video microscope (CVM) manufactured by SDL-UK, according to ASTM D724-99 (standard test method of surface wettability of paper) and ASTM D5946-96 (standard test method of corona-treated polymer films).

The contact angles determined, reported in Table 2, are the average values of at least three measurements. Atomic force microscopy (AFM) imaging of neat PVDF (sample M2) and PVDF blended with nano-silica (sample M6) was carried out with a Wet-SPM scanning probe microscope from Shimadzu. Scanned area was 2 μm × 2 μm and roughness in the range 0.9–7.2 Å. Zeta potentials were determined using streaming potential measurements apparatus SurPass electrokinetic analyzer from Anton Paar GmbH (Middle East Technical Centre). The test was repeated three times for each sample [19–21].

2.4. Determination of filtration and antifouling performance of membrane

Filtration and antifouling performances of UF membranes have been investigated with a laboratory testing apparatus, consisting of a flat sheet membrane module connected to a pressure pump and a 5 L feed tank. The experiments were carried out at ambient temperature, operating pressure of 8 bar and the effective surface area of UF membrane was 19.6 cm². All experiments were repeated three times for each sample.

Permeate flux (J) crossing the membrane was calculated with the following equation [5,11]:

$$J \left(\frac{\text{kg}}{\text{m}^2 \cdot \text{h}} \right) = \frac{Q}{A \cdot t} \quad (2)$$

where, Q is the mass of permeate (reported in kg), A is the active surface area of membrane (m^2), and t (h) the permeation time.

R represents the rejection degree calculated according to the following equation [11]:

$$R(\%) = \frac{C_f - C_p}{C_f} \times 100 \quad (3)$$

where C_f is the humic acid concentration (2, 5, and 10 g/L) of the feed solution and C_p the corresponding concentration in permeate.

For the determination of flux recovery ratio [F_{RR} , Eq. (4)], total fouling ratio [R_t , Eq. (5)], reversible fouling ratio [R_r , Eq. (6)], and irreversible fouling ratio [R_{ir} , Eq. (7)] were measured in sequence: (1) initial permeate flux of water (J_{W1}), via fluxing neat water for 1 h; (2) permeate fluxes (J_p), via fluxing for 1 h aqueous humic acid (10 g/L), or aqueous bovine serum albumin (BSA, 3 g/L); (3) final permeate flux of water (J_{W2}), via fluxing neat water for 1 h. All experiments were repeated three times, washing the membrane for 300 min with water after each sequence of experiments. Below reported equations were used for determination of those parameters:

$$F_{RR}(\%) = \frac{J_{W2}}{J_{W1}} \times 100 \quad (4)$$

$$R_t(\%) = \left(1 - \frac{J_p}{J_{W1}}\right) \times 100 \quad (5)$$

$$R_r(\%) = \left(\frac{J_{W2} - J_p}{J_{W1}}\right) \cdot 100 \quad (6)$$

$$R_{ir}(\%) = \left(\frac{J_{W1} - J_{W2}}{J_{W1}}\right) \cdot 100 \quad (7)$$

3. Results and discussion

3.1. Membrane preparation

Mesoporous silica was prepared according to a conventional hydrothermal method [8]. TEOS and CTAB were used respectively as silicon source and templating agent. The molar ratio $SiO_2/CTABr/NaOH/EtOH/H_2O$ adopted for the synthesis was 1.4:1:0.35:5:140. The gel resulting from the synthetic procedure was treated at 373 K for 4 d into a teflon-lined stainless-steel autoclave. The intermediate product, after recovery via filtration and washing, was calcined in air. The functionalization with amine groups was then accomplished by treatment of the silica with the amine silane, dispersed in toluene under protective atmosphere of argon, followed by annealing at 383 K. The final product was recovered by conventional filtration, washing, and drying.

Poly(vinylidene fluoride)-nano-silica (PVDF-NS) ultra-filtration (UF) membranes were subsequently prepared via compounding in N-methyl-2-pyrrolidone (NMP) of PVDF, PEG, and NS (suspended in dodecyl amine/ethanol solvent mixture) followed by casting onto woven or nonwoven supports. The concentration of NS adopted for membrane production are reported in Table 1.

3.2. X-ray diffraction and transmission electron microscopy of amino-functionalized nano-silica

The XRD diffraction pattern of a representative mesoporous silica sample after the synthetic procedure adopted for the functionalization with amino groups is reported in Fig. 1. The broad reflection centered at 2θ of 23° is diagnostic for an amorphous sample, in conformity with published literature for amino silylated MCM-48 [22]. The typical diffraction pattern for a cubic structure, correlated to the space group Ia3d for MCM-48, was lost after functionalization.

TEM micrograph in Fig. 2 provides information on the nanoparticle size and shows a nanostructure with pore distance of about 1.5 nm, in agreement with an amino-silylated silica previously reported in literature [23].

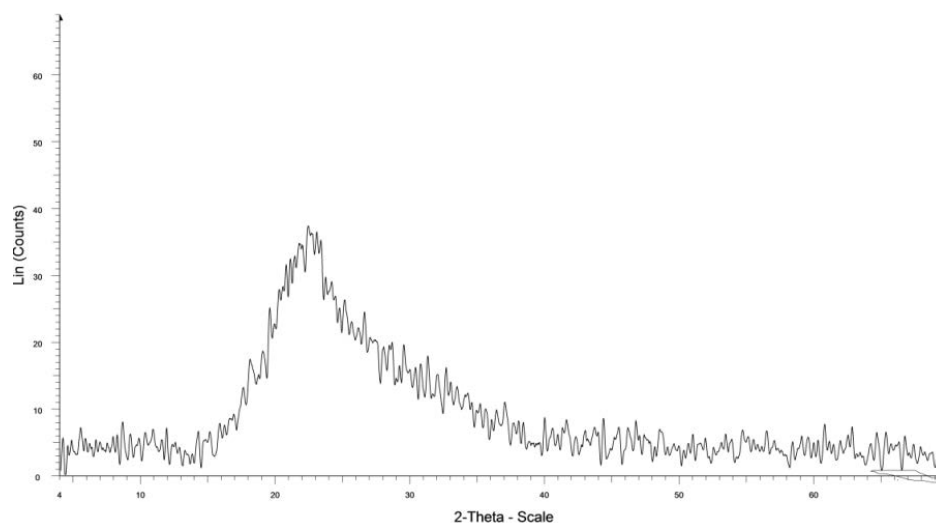


Fig. 1. XRD pattern for the powder of amino-functionalized nano-silica.

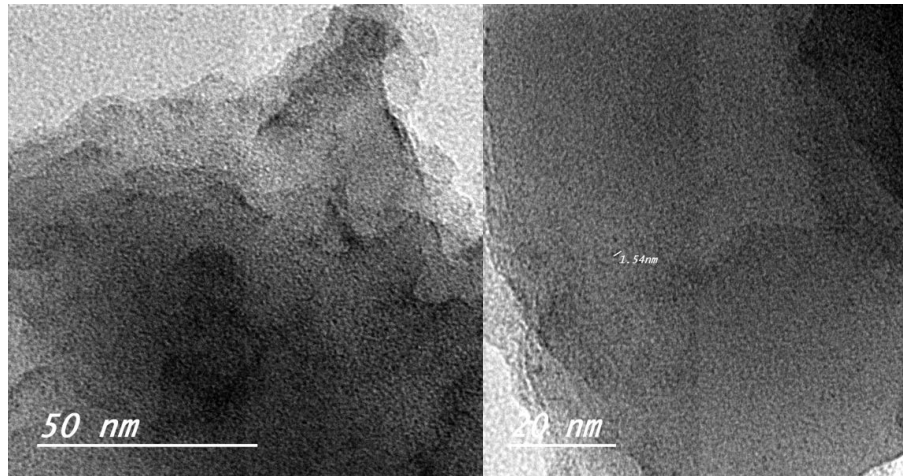


Fig. 2. TEM micrographs of amino-functionalized nano-silica.

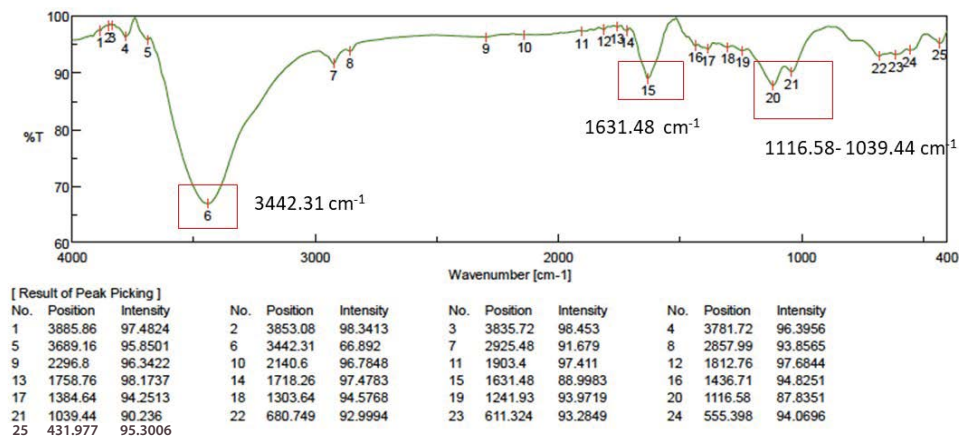


Fig. 3. FTIR for pristine nano-silica.

3.3. FTIR spectroscopy of amino-functionalized nano-silica

Fig. 3 shows the infrared spectra of mesoporous nano-silica before functionalization with amino groups. The bands around 473; 795; 1,080; and 1,220 cm^{-1} are assigned to Si–O–Si bonds of silica [24]. The wide absorption band centered at 3,431 cm^{-1} can be ascribed to hydrogen-bonding in Si–OH groups. The peak at the 3,442 cm^{-1} can be assigned to the vibration of single Si–OH moiety. That band resulted strongly attenuated after functionalization (compare Figs. 3 and 4), indicating the involvement of Si–OH moieties in the grafting of the amino silane. The grafting was also confirmed by the emergence of absorption bands at 3,368–3,298 cm^{-1} and 1,630–1,478 cm^{-1} due to N–H bonds (amino groups) and at 2,931–2,869 cm^{-1} for C–H groups bonding [25]. In addition, further bands at wavenumber of 1,094 and 468 cm^{-1} resulted in an agreement with published data on amino-functionalized silica [26].

3.4. Scanning electron microscopy

SEM micrographs of cross-section of M1–M8 UF membranes are reported in Fig. 5. Figs. 5a and b, show a

finger-like structure for the top layer and a compact structure for the bottom layer both for M1 and M2 membranes prepared in absence of silica, respectively, deposited onto nonwoven and woven support, although larger pores can be observed for the latter membrane. Figs. 5c and d report representative morphologies for PVDF membrane where 0.1 wt.% of nano-silica were used during membrane preparation. Both the structures resulted compact with greater penetration of the polymer-silica composite in the woven support (Fig. 5d). Increasing the silica content to 0.3 wt.% during membrane preparation, resulted into a compact morphology for the membrane deposited onto nonwoven support (Fig. 5e), and on the contrary, into a well-defined finger-like structure with high porosity for the corresponding deposited on woven support (Fig. 5f). Finally, a further increasing of silica content to 0.5 wt.% (Figs. 5g and h) resulted in thicker membrane layers for both the substrates. Both the structure for these latter membranes resulted sponge-like, with higher porosity for the membrane deposited onto woven support (compare Figs. 5g and h). Increasing the nano-silica content leads to an increase in viscosity with a resulting delay in demixing of the polymer during coagulation step, leading to the formation of a thicker layer of the

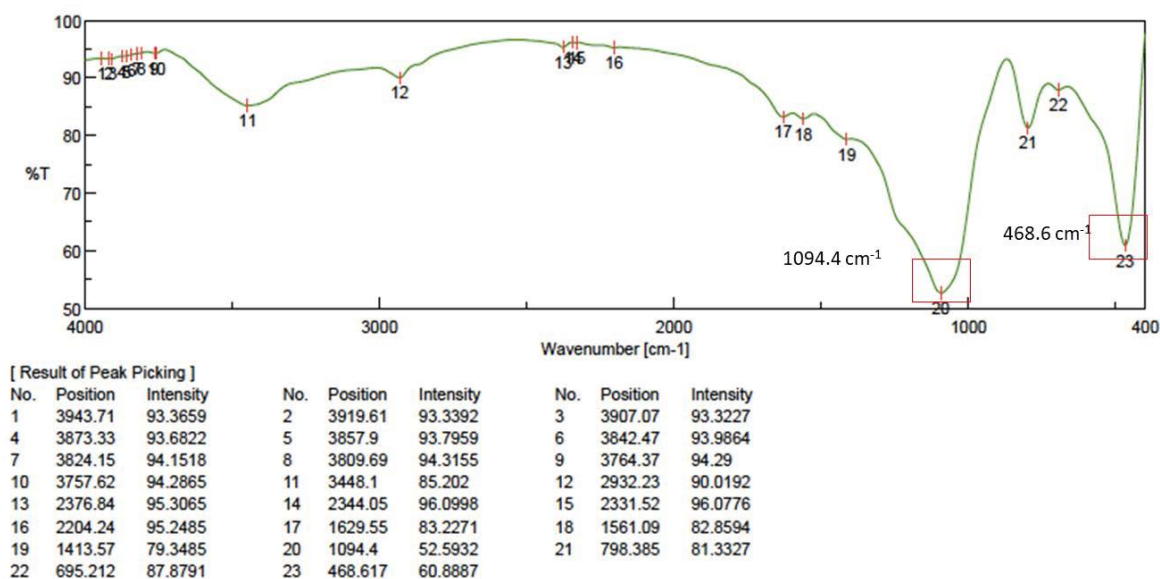


Fig. 4. FTIR for amino-functionalized nano-silica.

polymer solution. All membranes prepared did not showed silica aggregates in micrometer size [27,28].

3.5. Atomic force microscopy

Atomic force microscopy (AFM) is a powerful tool for the identification of surface morphology and phase separations in polymer composites [7,29–36]. Morphology of *M2* and *M6* membranes, consisting respectively of PVDF and PVDF compounded with 0.3% of nano-silica during membrane preparation (Table 1), was further investigated by AFM with purpose to explore surface topography. Roughness parameters and height AFM micrographs for *M2* and *M6* are respectively reported in Table 2 and Fig. 6. The surface of the membrane *M6*, containing nano-silica, resulted homogeneous; without raw phase separations in the micrometre scale: as a further evidence of the optimal compounding of the polymer with the filler (Fig. 7). Both the membranes presented smooth surfaces with similar roughness parameters (Table 2).

3.6. Tensile properties of membrane

Tensile properties of *M1*–*M8* membranes were investigated and reported in Fig. 7. *M5* and *M6*, respectively membrane composed of PVDF with 0.3 wt.% nano-silica on non-woven and woven support, showed the highest tensile strength. A tensile strength of 82.5 Kg/m² and elongation at break of 25.5% were found for *M5*, while for *M6* the same parameters were respectively 87.9 kg/m² and 29.3%. Fig. 7 indicates that the increasing of nano-silica content leads to an improvement in the tensile strength due to dispersion of the nano-silica as a filler in the polymer matrix, as an indication that the PVDF chains strongly interacts with nano-silica particles. Thus, SiO₂ can be effectively used as a filler for prepared membranes. The high rigidity of the nano-silica leads to an increased reinforcement of the final composite,

resulting into an overall improvement of the mechanical properties. Tensile strength improvement is also due to reduction of polymer chain mobility, which depends on the intermolecular interaction with the reinforcing nanoparticles [11,37–42].

An increasing of nano-silica content up to 0.5 wt.% led to the formation of a more rigid membrane that, however, allow to preserve a high degree of PVDF crystallization with an overall benefit on the mechanical properties. Further increasing in silica content can afford higher nanoparticles aggregation, which produces stress points in membrane that can originate numbers of invisible microcracks with resulting worsening of mechanical properties [43,44]. On the other hand, the adoption of a woven support results into a more elastic membrane where the layers are mutually linked to each other, contrarily to non-woven support with unlinked layers.

3.7. Wettability of membrane

Information on membrane hydrophilicity, that is, on its wettability, can be obtained by measurement of contact angle between its surface and a deposited droplet of water. The results indicated that an increase of nano-silica leads to improvements in membrane hydrophilicity (Table 3). The highest contact angles of 98.3° and 123.5° were found for pure PVDF, that is, for membrane *M1* and *M2*. On the contrary, membranes *M7* and *M8*, with the highest silica content, showed the lowest values of contact angle, respectively of 63.7° and 73.7°. Hydroxyl groups on silica surface contribute to improving membrane hydrophilicity [18–27], with resulting reduction of contact angle as reported in Table 2. The results also indicate that increasing of nanoparticles decreased the porosity of prepared membranes due to the formation of the skin layer on the top of the membrane and reducing the size of the pores of the membrane as shown in Table 3. In addition, can be observed that membranes

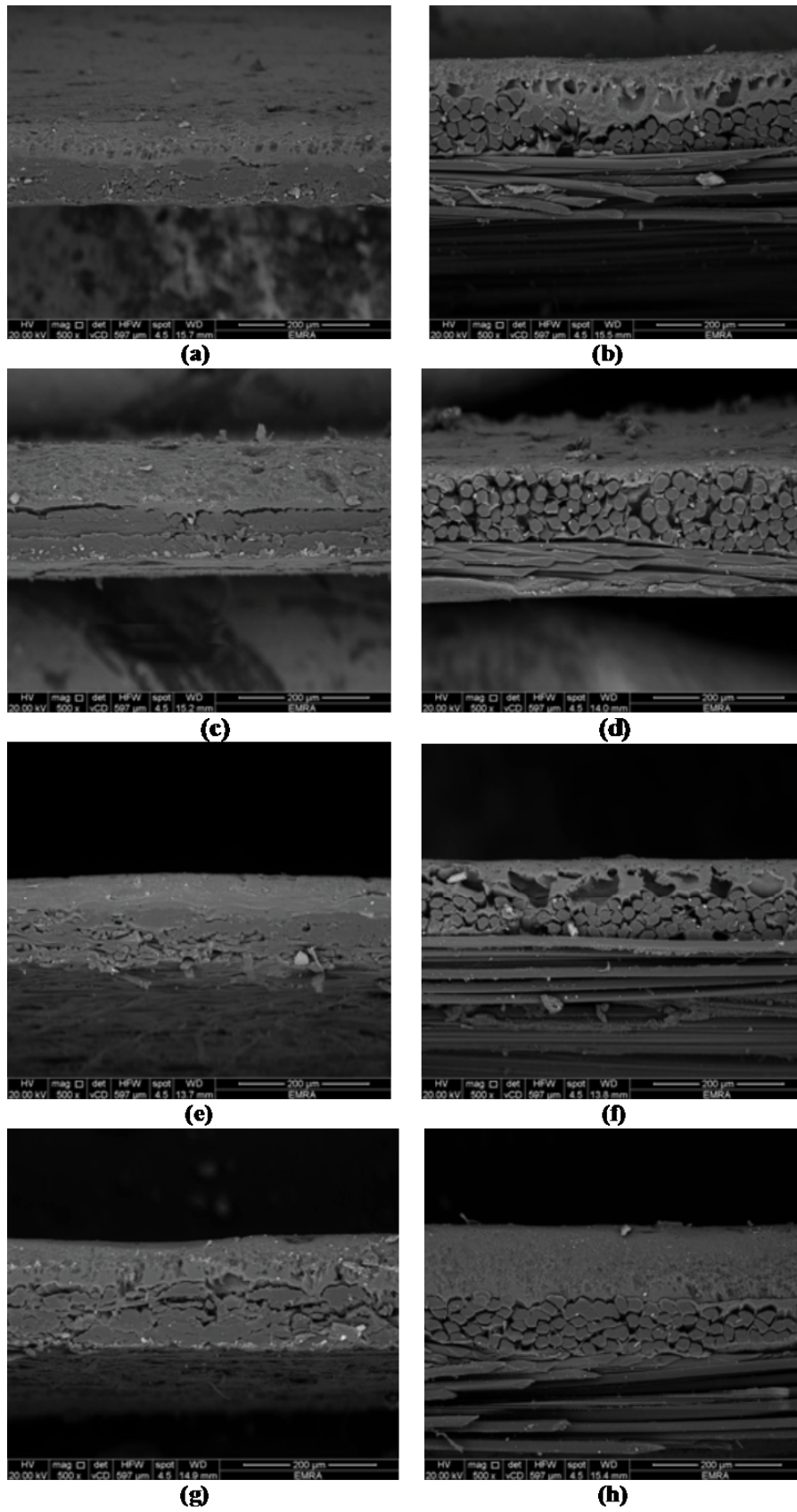


Fig. 5. SEM micrographs of membranes (a) M1, (b) M2, (c) M3, (d) M4, (e) M5, (f) M6, (g) M7, and (h) M8 (Table 1).

Table Table 2
Roughness parameters of M2 and M6 membranes determined by AFM

Membrane	Mean rough surface area (μm^2)	Roughness (μm)	Average peak heights (μm)
M2	0.262 ± 1.5	1.51 ± 1.1	345.5
M6	0.177 ± 1.2	1.48 ± 0.76	315.9

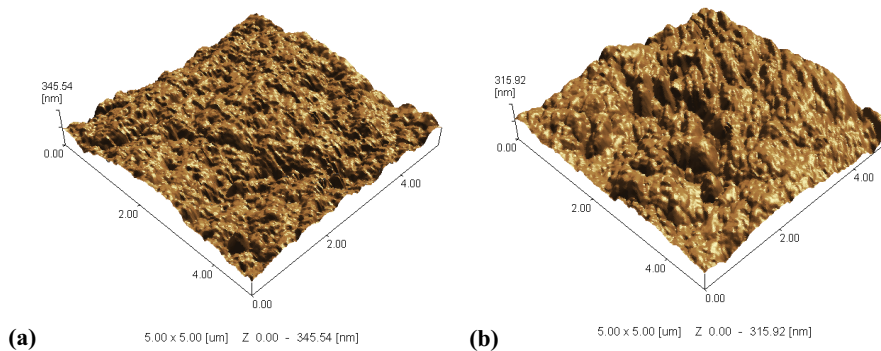


Fig. 6. AFM height images of membrane M2 (a) and M6 (b).

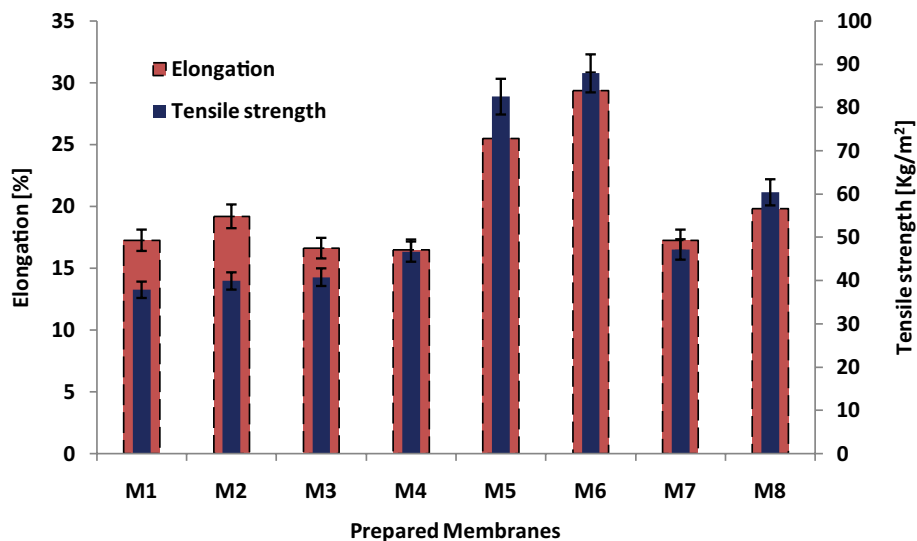


Fig. 7. Mechanical properties of prepared membranes.

prepared by casting on non-woven support show a higher contact angle when compared with the membranes prepared on the woven support. The polymeric-silica suspension during membrane casting penetrates the voids between the fibers in the woven support leading to membranes with high thickness and the hydrophobicity of the fibers can affect the hydrophilicity of the membrane surface [9,43].

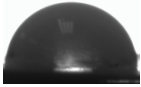
3.8. Surface area and pore analysis according to BET model

The inner surface area of M1–M8 membranes was determined and reported in Table 3. The addition of nano-silica regulates the viscosity of the polymeric suspension during

membrane preparation. The rate of formation of the skin top layer of membrane, as well as the rate of polymer coagulation are both depending on the viscosity of the polymer-silica suspension [11,40–44]. M3 and M4, prepared with 0.1 wt.% of nano-silica in the polymeric solution, showed a mean diameter of pores decreased with respect to that of M1 and M2 due to the increase in the size of skin top layer.

The use of 0.3 wt.% of nano-silica increases the polymeric solution viscosity, that leads to a slowdown in phase separation, which prevents the formation of large pores. Therefore, the prepared membranes resulted more compact and with uniform distribution of small pores with higher internal surface area and improved porosity

Table 3
Contact angle and porosity for prepared membranes

Membrane	Contact angle (°)	Porosity (%)	Membrane wet ability
M1	123.5 ± 0.5	44.4 ± 0.5	
M2	98.5 ± 1.1	15.3 ± 0.25	
M3	66.6 ± 1	20.8 ± 0.2	
M4	77.4 ± 1.5	18.3 ± 0.3	
M5	62.2 ± 1.2	25.4 ± 0.23	
M6	76.6 ± 1.1	19.9 ± 0.5	
M7	63.7 ± 0.7	33.7 ± 0.34	
M8	73.7 ± 1.2	25.3 ± 0.33	

(Table 4). A further increase of the nanosilica content to 0.5 wt.% (membranes M7 and M8) leads to highly viscous polymeric solutions, that further delayed the phase separation process during membrane formation, with resulting reduction in pore size. On the other hand, the coagulation of the highly viscous solutions can afford heterogeneous pore distributions due to the strong delay in the exchange between solvent and non-solvent during membrane formation [8,13]. Hence, the high number of pores with small volume results in a higher membrane porosity [16,17].

3.9. Zeta potential of membrane

Fig. 8 shows the zeta potential of the prepared PVDF/nano-silica blend membranes. Fig. 8a illustrates zeta potential for prepared membranes on woven support, while Fig. 8b indicates zeta potential for prepared membranes on non-woven support. The isoelectric point of pure PVDF membrane without any addition using woven support is 5.01 (M1), while pure PVDF using non-woven is presented negative charge for all pH ranges (M2). Isoelectric point (IEP) for PVDF/0.1 NS using woven support is 5.07 (M3) while using nonwoven support the IEP is 6.07 (M4).

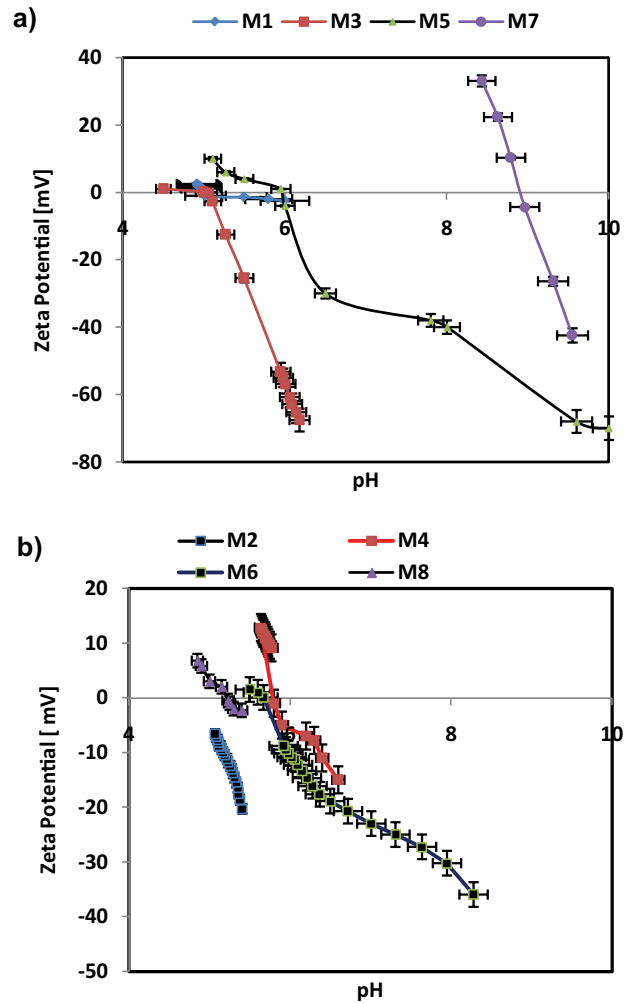


Fig. 8. Zeta potential as a function of pH of membranes deposited on: (a) woven support and (b) non-woven support.

However, IEP for PVDF/0.3 NS (M5) using woven support is 5.94 and IEP using nonwoven support (M6) is 5.67. Also, (M7) IEP for PVDF/0.5 NS using woven support is 8.91 and (M8) IEP using nonwoven support is 5.15. The positive charge is appeared according to $-NH_2$ groups protonation when the $pH < \text{isoelectric point}$, but the negative charge appears when $pH > \text{isoelectric point}$ due to the deprotonation of amine functional groups and dissociation of $-COOH$ group.

Woven support is a satin this kind of fabric composed of several amino acids, mostly glycine, alanine, and serine. It has the smallest side chains, leading to the stack of the fabric chains neatly together, which leads to the smooth surface of satin and strong intermolecular forces between the stacked and planar sheets in case of pure PVDF membrane which supported by woven support has isoelectric point 5.01, while PVDF membrane has a negative charge because nonwoven support is formed from polyester [44]. Polyester (PET) consists of repeating a linear unit of an aromatic ring that was attached to either side to the carbonyl group then it stretched on one side to two CH_2 groups.

Table 4
Measurement of BET area and pores characterization

Membrane	BET area (m ² /g)	Total pore volume (cm ³ /g)	Mean pore diameter (nm)
M1	1.6 ± 0.5	5.1 × 10 ⁻³ ± 0.5	12.5 ± 0.5
M2	3.6 ± 0.5	6.8 × 10 ⁻³ ± 0.5	7.5 ± 0.5
M3	4.40 ± 0.25	9.9 × 10 ⁻³ ± 0.25	9.0 ± 0.25
M4	3.68 ± 0.34	7.11 × 10 ⁻³ ± 0.34	6.73 ± 0.34
M5	4.25 ± 0.2	1.025 × 10 ⁻³ ± 0.2	8.64 ± 0.2
M6	5.91 ± 0.5	7.83 × 10 ⁻³ ± 0.5	5.6 ± 0.5
M7	2.17 ± 0.43	3.87 × 10 ³ ± 0.43	7.12 ± 0.43
M8	4.12 ± 0.25	5.46 × 10 ⁻³ ± 0.25	5.29 ± 0.25

Polyester has the ability to acids resistance, but it could be attacked by alkali. The aromatic ring of polyester provides rigidity structure and reduce the deforming and wrinkle-resistant for membranes [45].

3.10. Membrane performance

Humic acid solutions of 3, 5, and 10 g/L were used for testing of membrane performance. Figs. 9 and 10 show the performance of prepared membranes in terms of humic acid rejection percentage and permeate flux respectively. The experiments were performed under an operating pressure of 8 bar using different humic acid concentrations to determine the applicability of these membranes in the ultrafiltration process. It is clear from Figs. 9 and 10 that among the investigated membrane, M5 and M6 showed higher performance, on the base of rejection percentage and permeate flux. Nano silica 0.3 wt.% was used in the membrane formation step of M5 and M6, where the membrane prepared using this percentage exhibits good morphology due to the formation of the small dense top layer and wide finger like in the sub-layer especially at M6 using woven support. M5 exhibits the best rejection 99.7% for removal of humic acid concentration 3 g/L with permeate flux 294 L/m²h and M6

provides best permeate flux 347 L/m²h with rejection 98.8% for removal of humic acid concentration 3 g/L. According to zeta potential test, the humic acid solution has a negative charge at pH7 and M5 and M6 have negative charge surface. So, humic acid was excluded due to electrostatic repulsion and the membranes exhibited high water permeability and high removal percentage compared with other membranes [46]. M7 and M8 provide good removal percentage but there was a reduction in the flux because the membrane surface in M7 and M8 has two charges positive and negative in the pH 7, that leading to adsorption of the humic acid on the surface and make a fouling on positive parts on the surface.

The BSA was studied in the removal test using a feed concentration of 3 g/L as shown in Fig. 11. The results indicate that M5 and M6 provide the highest removal of the bovine serum albumin, which was 99.5% for M5 and 99.2% for M6 with permeate flux 332.2 and 392.6 L/m²h for M5 and M6, respectively. According to the zeta potential test, these membranes carry a negative charge and BSA has a negative charge, so the albumin doesn't precipitate on the membrane surface as a result of repulsion of charges, which make pores feel free from clogging of the pores compared with M7 and M8 which have a positive charge on the membrane surface, so the membranes were fouled, leading to low permeate flux

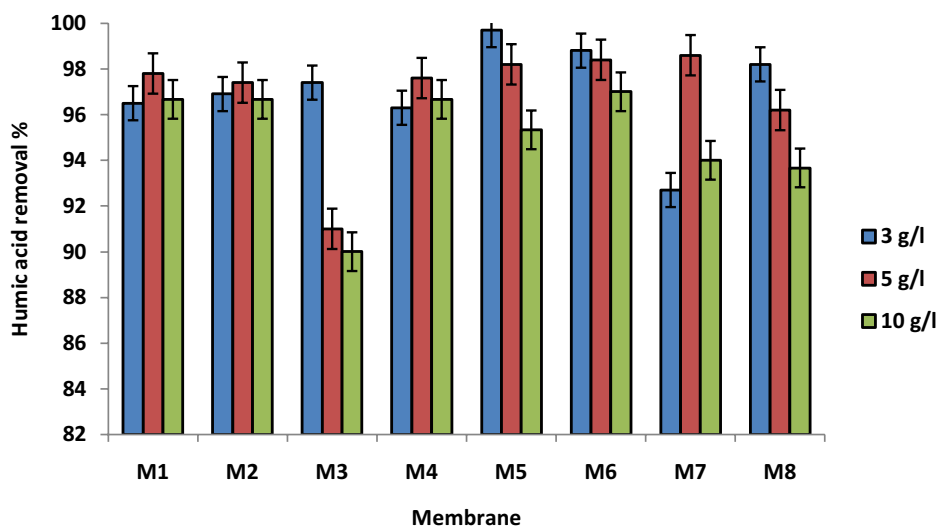


Fig. 9. Humic acid removal using prepared membranes as a function in different humic acid concentrations.

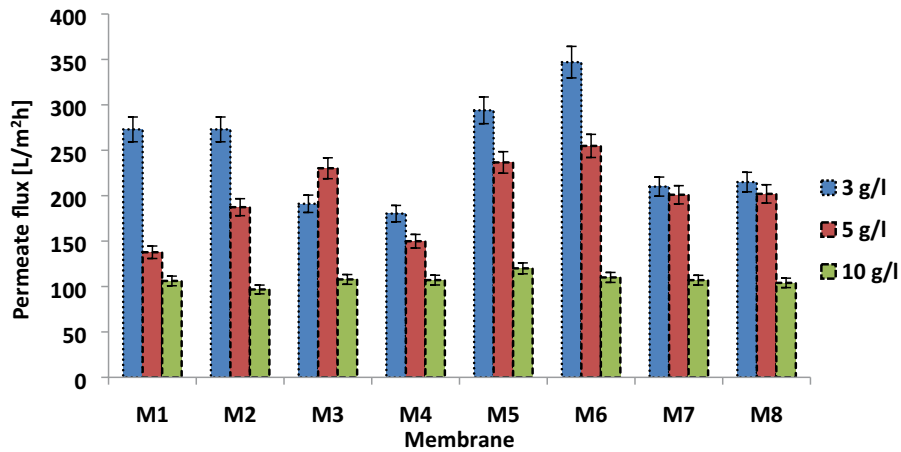


Fig. 10. Permeate flux using prepared membranes as a function in different humic acid concentrations.

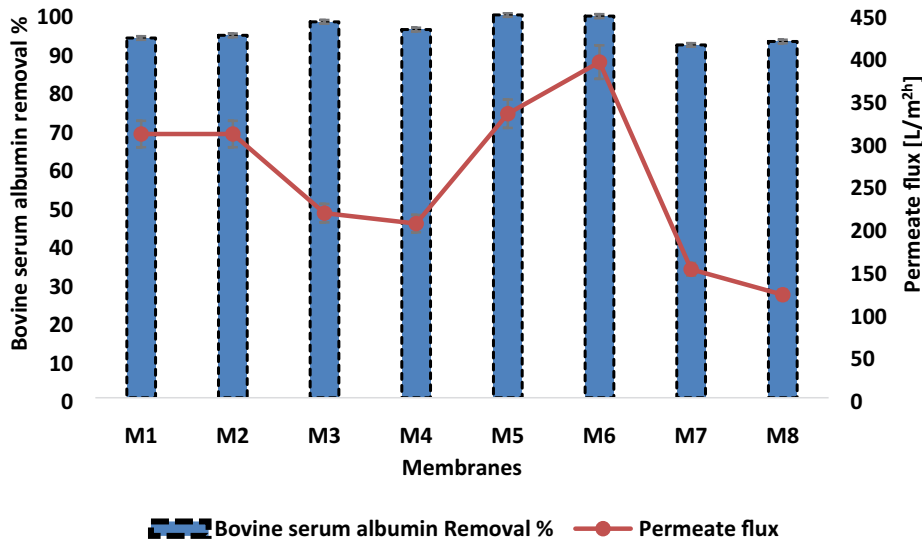


Fig. 11. Membrane performance using bovine serum albumin in the feeding solution.

[47]. However, the percentage of nano-silica solution which contains dodecyl amine which is a surfactant helps in anti-fouling properties, so increasing the percentage of NS to 0.3 wt.% enhances the membrane performance.

3.11. Anti-fouling properties of membrane

The anti-fouling test was applied on prepared membranes M1–M8 (by determination of water flux recovery after passing the humic acid solution (10 g/L) and bovine serum (3 g/L) on membranes, respectively. Table 5. illustrates that antifouling parameters like F_{RR} , R_r , and R_{ir} . The F_{RR} of M5 was 99.71%, while F_{RR} for M6 was 99.43%. The F_{RR} shows excellent antifouling property for the membranes M5 and M6. The results indicate that reversible fouling on the membrane surface due to the adsorption or deposition of humic acid molecules, which was easily removed by back-wash. M5 has R_r ; 10.7% and M6 has R_r ; 11.8%. However,

irreversible fouling was formed according to clogging the membrane pores, where R_{ir} was 0.28% for M5 and 0.57% for M6 and R_i was 10.9% for M5 and 12.4% for M6. The results indicated that very low irreversible resistance, which means a low amount of humic acid molecules were clogged the pores [28,37,48,49]. The negative charge in the membrane surface makes hindrance for the molecules of humic acid to pass through membranes pores, which leads to improve F_{RR} and reduce the R_{ir} [46].

The fouling test was repeated using BSA (3 g/L). Table 5 indicates the fouling test for all prepared membranes using bovine serum albumin. The results indicate that F_{RR} for M5 was 98.5% and M6 was 97.96%. The adsorption of BSA on the membrane surface causes reversible fouling, where R_r was 10.93% for M5 and 6.87% for M6. However, irreversible fouling R_{ir} was 1.5% for M5 and 2.04% for M6. The results indicated that very low irreversible resistance for M5 and M6 compared with other membranes. Using nano-silica solution

Table 5
Antifouling parameters results using feeding solution from humic acid and bovine serum albumin

Foulant Membranes	Humic acid			Bovine serum albumin		
	R_{ir} %	R_r %	F_{RR} %	R_{ir} %	R_r %	F_{RR} %
M1	1.13 ± 0.2	42.94 ± 0.2	83.09 ± 0.2	6.03 ± 0.1	43.72 ± 0.1	89.54 ± 0.1
M2	2.28 ± 0.12	47.29 ± 0.12	82.85 ± 0.12	8.14 ± 0.15	27.48 ± 0.15	85.19 ± 0.15
M3	0.85 ± 0.11	32.2 ± 0.11	97.76 ± 0.11	4.52 ± 0.14	32.79 ± 0.14	93.80 ± 0.14
M4	1.71 ± 0.2	35.47 ± 0.2	97.48 ± 0.2	6.11 ± 0.2	20.61 ± 0.2	92.42 ± 0.2
M5	0.28 ± 0.25	10.73 ± 0.25	99.72 ± 0.25	1.51 ± 0.16	10.93 ± 0.16	98.49 ± 0.16
M6	0.57 ± 0.22	11.82 ± 0.22	99.43 ± 0.22	2.04 ± 0.15	6.87 ± 0.15	97.96 ± 0.15
M7	1.98 ± 0.21	64.41 ± 0.21	90.65 ± 0.21	7.54 ± 0.2	54.65 ± 0.2	91.2 ± 0.2
M8	2.85 ± 0.15	59.12 ± 0.15	90.39 ± 0.15	10.18 ± 0.2	34.35 ± 0.2	90.71 ± 0.2

(3%) provide a negative charge surface that provides electrostatic repulsion for bovine serum albumin, which carried a negative charge, so these membranes are antifouling can be used for wastewater treatment especially for the waters contaminated by proteins [47].

4. Conclusion

Ultrafiltration membranes obtained by compounding polyvinylidene fluoride with functionalized mesoporous amino nano-silica were prepared using the phase inversion method. The following conclusions can be drawn from the present work:

- The prepared functionalized mesoporous amino nano-silica was characterized using XRD, TEM, and FTIR.
- The repaired membranes with functionalized mesoporous amino nano-silica have relatively dense and homogeneous structures and any apparent void when was used a non-woven support. Increasing in nano-silica percentage resulted in the formation of small voids in membrane structure when was adopted a woven support.
- Membrane M5 and M6 (PVDF membranes with 0.3 wt.% of nano-silica on non-woven support and woven support, respectively) showed the highest tensile strengths. M5 showed a tensile strength of 82.5 kg/m² and elongation of 25.5%, while M6 showed 87.9 kg/m² with elongation of 29.3%.
- Wettability tests explain that the incorporation of amino nano-silica in membrane enhances the hydrophilicity.
- AFM micrographs indicate that the M6 membrane is smoother than the pure PVDF membrane due to excellent contrast in pores distribution after blending with 0.3 wt.% nano-silica, leading to reduced surface roughness.
- Membrane performance tests indicate that the membrane M5 exhibits the best rejection 99.7% for removal of humic acid (concentration 3 g/L) with permeate flux 294 L/m²h and M6 afforded the best permeate flux 347 L/m²h with rejection 98.8% for removal of humic acid concentration 3 g/L.
- The removal of bovine serum albumin was studied using a feed concentration of 3 g/L. M5 and M6 membranes showed the highest performance in removal of bovine serum albumin, with degree of 99.5% for M5 and 99.2% for M6, with permeate flux 332.2 and 392.6 L/m²h for M5 and M6, respectively.

- Antifouling properties of membrane were investigated with solutions of humic acid (10 g/L) and bovine serum albumin (3 g/L). The membrane M5 and M6 showed excellent antifouling properties, with F_{RR} respectively of 99.71% and 99.43% for humic acid, and F_{RR} respectively of 98.5% and 97.96% for bovine serum albumin.

Acknowledgments

The research activities were partially funded by the National Research Centre for the STDF funded Italian Egyptian project no. 25920 linked to the international project no. EG16MO01 of the Italian ministry of foreign affairs. The authors gratefully thank the flat sheet membrane group colleague from a central laboratory in NRC for the cooperation and the precious help given during the research activity.

References

- [1] G.-d. Kang, Y.-m. Cao, Application and modification of poly(vinylidene fluoride) (PVDF) membranes – a review, *J. Membr. Sci.*, 463 (2014) 145–165.
- [2] F. Liu, N.A. Hashim, Y. Liu, M.R.M. Abed, K. Li, Progress in the production and modification of PVDF membranes, *J. Membr. Sci.*, 375 (2011) 1–27.
- [3] D. Rana, B.M. Mandal, S.N. Bhattacharyya, Miscibility and phase diagrams of poly(phenyl acrylate) and poly(styrene-co-acrylonitrile) blends, *Polymer*, 34 (1993) 1454–1459.
- [4] D. Rana, K. Bag, S.N. Bhattacharyya, B.M. Mandal, Miscibility of poly(styrene-co-butyl acrylate) with poly(ethyl methacrylate): existence of both UCST and LCST, *J. Polym. Sci., Part B: Polym. Phys.*, 38 (2000) 369–375.
- [5] D. Rana, B.M. Mandal, S.N. Bhattacharyya, Analogue calorimetric studies of blends of poly(vinyl ester)s and polyacrylates, *Macromolecules*, 29 (1996) 1579–1583.
- [6] A. El-Gendi, H. Abdallah, Thermodynamic modeling of polyamide-6 (PA-6)/cellulose acetate (CA) blend membrane prepared via casting technique, *J. Polym. Eng.*, 33 (2013) 701–712.
- [7] A. Buonerba, C. Cuomo, V. Speranza, A. Grassi, Crystalline syndiotactic polystyrene as reinforcing agent of cis-1,4-polybutadiene rubber, *Macromolecules*, 43 (2010) 367–374.
- [8] M. Baghbanzadeh, D. Rana, C.Q. Lan, T. Matsuura, Effects of hydrophilic silica nanoparticles and backing material in improving the structure and performance of VMD PVDF membranes, *Sep. Purif. Technol.*, 157 (2016) 60–71.
- [9] D. Hou, J. Wang, X. Sun, Z. Ji, Z. Luan, Preparation and properties of PVDF composite hollow fiber membranes for desalination through direct contact membrane distillation, *J. Membr. Sci.*, 405–406 (2012) 185–200.

- [10] M. Shaban, H. Hamdy, H. Abdallah, L. Said, A.A. khalek, Effects of TiO₂ NTs% on polyethersulfone/TiO₂ NTs membranes, *J. Mater. Sci. Eng., A*, 5 (2015) 65–68.
- [11] S.M. Ibrahim, H. Nagasawa, M. Kanezashi, T. Tsuru, Robust organosilica membranes for high temperature reverse osmosis (RO) application: membrane preparation, separation characteristics of solutes and membrane regeneration, *J. Membr. Sci.*, 493 (2015) 515–523.
- [12] V. Garcia-Molina, S. Lyko, S. Esplugas, T. Wintgens, T. Melin, Ultrafiltration of aqueous solutions containing organic polymers, *Desalination*, 189 (2006) 110–118.
- [13] L.-F. Fang, M.-Y. Zhou, L. Cheng, B.-K. Zhu, H. Matsuyama, S. Zhao, Positively charged nanofiltration membrane based on cross-linked polyvinyl chloride copolymer, *J. Membr. Sci.*, 572 (2019) 28–37.
- [14] L. Zhu, H. Song, D. Zhang, G. Wang, Z. Zeng, Q. Xue, Negatively charged polysulfone membranes with hydrophilicity and antifouling properties based on in situ cross-linked polymerization, *J. Colloid Interface Sci.*, 498 (2017) 136–143.
- [15] X. Wang, G.Q. Chen, W. Zhang, H. Deng, Surface-modified anion exchange membranes with self-cleaning ability and enhanced antifouling properties, *J. Taiwan Inst. Chem. Eng.*, 105 (2019) 8–16.
- [16] A. Ahmadi, O. Qanati, M.S. Seyed Dorraji, M.H. Rasoulifard, V. Vatanpour, Investigation of antifouling performance a novel nanofibrous S-PVDF/PVDF and S-PVDF/PVDF/GO membranes against negatively charged oily foulants, *J. Membr. Sci.*, 536 (2017) 86–97.
- [17] H. Abdallah, M. Shalaby, M. Saad, A. Shaban, Supporting polyvinylchloride polymeric blend membrane with coated woven fabric, *J. Membr. Sci. Res.*, 4 (2018) 174–180.
- [18] H. Abdallah, M.S. Shalaby, A.M.H. Shaban, Performance and characterization for blend membrane of PES with manganese(III) acetylacetonate as metalorganic nanoparticles, *Int. J. Chem. Eng.*, 2015 (2015) 1–9, doi: 10.1155/2015/896486.
- [19] J.C. Wang, P. Chen, L. Chen, K. Wang, H. Deng, F. Chen, Q. Zhang, Q. Fu, Preparation and properties of poly(vinylidene fluoride) nanocomposites blended with graphene oxide coated silica hybrids, *Express Polym. Lett.*, 6 (2012) 299–307.
- [20] M.R. Bilad, E. Guillen-Burrieza, M.O. Mavukkandy, F.A. Al Marzooqi, H.A. Arafat, Shrinkage, defect and membrane distillation performance of composite PVDF membranes, *Desalination*, 376 (2015) 62–72.
- [21] S. Sahebi, S. Phuntsho, L. Tijing, G. Han, D.S. Han, A. Abdel-Wahab, H.K. Shon, Thin-film composite membrane on a compacted woven backing fabric for pressure assisted osmosis, *Desalination*, 406 (2017) 98–108.
- [22] Q.H. Xia, K.X. Su, X.T. Ma, H.Q. Ge, H.B. Zhu, Efficiently tailoring the pore diameter of mesoporous MCM-48 to micropore, *Mater. Lett.*, 59 (2005) 2110–2114.
- [23] K. Schumacher, P.I. Ravikovitch, A. Du Chesne, A.V. Neimark, K.K. Unger, Characterization of MCM-48 materials, *Langmuir*, 16 (2000) 4648–4654.
- [24] S. Rita, R. Eti, K. Tetty, Aminopropyltrimethoxysilane (APTMS) modified nano silica as heavy metal iron (Fe) adsorbents in peat water, *AIP Conf. Proc.*, 2014 (2018) 020163-1–020163-6, doi: 10.1063/1.5054567.
- [25] R. Yuvakkumar, V. Elango, V. Rajendran, N. Kannan, High-purity nano silica powder from rice husk using a simple chemical method, *J. Exp. Nanosci.*, 9 (2014) 272–281.
- [26] P. Taba, P. Budi, A.Y. Puspitasari, Adsorption of heavy metals on amine-functionalized MCM-48, *IOP Conf. Ser.: Mater. Sci. Eng.*, 188 (2017) 1–9, doi: 10.1088/1757-899X/188/1/012015.
- [27] A. El-Gendi, H. Abdallah, A. Amin, S.K. Amin, Investigation of polyvinylchloride and cellulose acetate blend membranes for desalination, *J. Mol. Struct.*, 1146 (2017) 14–22.
- [28] S. Kang, A. Asatekin, A.M. Mayes, M. Elimelech, Protein antifouling mechanisms of PAN UF membranes incorporating PAN-g-PEO additive, *J. Membr. Sci.*, 296 (2007) 42–50.
- [29] A. Buonerba, V. Speranza, A. Grassi, Novel synthetic strategy for the sulfonation of polybutadiene and styrene-butadiene copolymers, *Macromolecules*, 46 (2013) 778–784.
- [30] C. Capacchione, A. De Roma, A. Buonerba, V. Speranza, S. Milione, A. Grassi, Syndiotactic polystyrene-block-poly(methyl methacrylate) copolymer via click chemistry, *Macromol. Chem. Phys.*, 214 (2013) 1990–1997.
- [31] A. Buonerba, V. Speranza, P. Canton, C. Capacchione, S. Milione, A. Grassi, Novel nanostructured semicrystalline ionomers by chemoselective sulfonation of multiblock copolymers of syndiotactic polystyrene with polybutadiene, *RSC Adv.*, 4 (2014) 60158–60167.
- [32] N. Galdi, A. Buonerba, P. Oliva, L. Oliva, Nanostructured ethylene-styrene copolymers, *Polym. Chem.*, 5 (2014) 3045–3052.
- [33] M. Naddeo, A. Buonerba, E. Luciano, A. Grassi, A. Proto, C. Capacchione, Stereoselective polymerization of biosourced terpenes β -myrcene and β -ocimene and their copolymerization with styrene promoted by titanium catalysts, *Polymer*, 131 (2017) 151–159.
- [34] A. Buonerba, V. Speranza, C. Capacchione, S. Milione, A. Grassi, Improvement of tensile properties, self-healing and recycle of thermoset styrene/2-vinylfuran copolymers via thermal triggered rearrangement of covalent crosslink, *Eur. Polym. J.*, 99 (2018) 368–377.
- [35] A. Buonerba, F.D. Monica, V. Speranza, C. Capacchione, S. Milione, A. Grassi, Thin-film nanostructure and polymer architecture in semicrystalline syndiotactic poly(p-methylstyrene)-(cis-1,4-polybutadiene) multiblock copolymers, *Polym. Int.*, 68 (2019) 1681–1687.
- [36] D.H. Lamparelli, V. Speranza, I. Camurati, A. Buonerba, L. Oliva, Synthesis and characterization of syndiotactic polystyrene-polyethylene block copolymer, *Polymers*, 11 (2019) 1–11, doi: 10.3390/polym11040698.
- [37] S.S. Madaeni, N. Ghaemi, Characterization of self-cleaning RO membranes coated with TiO₂ particles under UV irradiation, *J. Membr. Sci.*, 303 (2007) 221–233.
- [38] L. Yu, K. Dean, L. Li, Polymer blends and composites from renewable resources, *Prog. Polym. Sci.*, 31 (2006) 576–602.
- [39] A.V.R. Reddy, H.R. Patel, Chemically treated polyethersulfone/polyacrylonitrile blend ultrafiltration membranes for better fouling resistance, *Desalination*, 221 (2008) 318–323.
- [40] Y. Zhao, C. Qiu, X. Li, A. Vararattanavech, W. Shen, J. Torres, C. Hélix-Nielsen, R. Wang, X. Hu, A.G. Fane, C.Y. Tang, Synthesis of robust and high-performance aquaporin-based biomimetic membranes by interfacial polymerization-membrane preparation and RO performance characterization, *J. Membr. Sci.*, 423–424 (2012) 422–428.
- [41] M. Mulder, Characterisation of Membranes, In: *Basic Principles of Membrane Technology*, Springer, Dordrecht, 1996, pp. 157–209.
- [42] X. Huang, J. Zhang, W. Wang, Y. Liu, Z. Zhang, L. Li, W. Fan, Effects of PVDF/SiO₂ hybrid ultrafiltration membranes by sol-gel method for the concentration of fennel oil in herbal water extract, *RSC Adv.*, 5 (2015) 18258–18266.
- [43] W. Li, X. Sun, C. Wen, H. Lu, Z. Wang, Preparation and characterization of poly(vinylidene fluoride)/TiO₂ hybrid membranes, *Front. Environ. Sci. Eng.*, 7 (2013) 492–502.
- [44] A. Cui, Z. Liu, C. Xiao, Y. Zhang, Effect of micro-sized SiO₂-particle on the performance of PVDF blend membranes via TIPS, *J. Membr. Sci.*, 360 (2010) 259–264.
- [45] X. Yang, B. Deng, Z. Liu, L. Shi, X. Bian, M. Yu, L. Li, J. Li, X. Lu, Microfiltration membranes prepared from acryl amide grafted poly(vinylidene fluoride) powder and their pH sensitive behaviour, *J. Membr. Sci.*, 362 (2010) 298–305.
- [46] L.-L. Hwang, H.-H. Tseng, J.-C. Chen, Fabrication of polyphenylsulfone/polyetherimide blend membranes for ultrafiltration applications: the effects of blending ratio on membrane properties and humic acid removal performance, *J. Membr. Sci.*, 384 (2011) 72–81.
- [47] L. Ghalamchi, S. Aber, V. Vatanpour, M. Kian, A novel antibacterial mixed matrixed PES membrane fabricated from embedding aminated Ag₂PO₄/g-C₃N₄ nanocomposite for use in the membrane bioreactor, *J. Ind. Eng. Chem.*, 70 (2019) 412–426.
- [48] E. Saljoughi, T. Mohammadi, Cellulose acetate (CA)/polyvinylpyrrolidone (PVP) blend asymmetric membranes: preparation, morphology and performance, *Desalination*, 249 (2009) 850–854.
- [49] R. Uma Maheswari, M.O. Mavukkandy, U. Adhikari, V. Naddeo, J. Sikder, H.A. Arafat, Synergistic effect of humic acid on alkali pretreatment of sugarcane bagasse for the recovery of lignin with phenomenal properties, *Biomass Bioenergy*, 134 (2020) 105486.